ORIGINAL PAPER

A highly efficient and accurate new SAV approach for the modified phase field crystal model

Zhengguang Liu[1] · **Nan Zheng**[2] · **Zhaojie Zhou**[1]

Abstract

The modified phase field crystal (MPFC) model is a sixth-order evolutive nonlinear partial differential equation which can describe many crystal phenomena. In this paper, we propose a highly efficient and accurate numerical method to construct linear and unconditionally energy stable schemes for the MPFC model. In recent years, the scalar auxiliary variable (SAV) and SAV-based methods have attracted much attention in numerical solution for dissipative systems due to their inherent advantage of preserving certain discrete analogues of the energy dissipation law. The considered numerical schemes are based on a new SAV-type approach which named new scalar auxiliary variable (nSAV) approach. We first give a first-order energy stable numerical scheme by introducing a new SAV $R(t)$. Then, the high-order nSAV schemes based on the k-step backward differentiation formula (BDFk) are constructed. The considered nSAV schemes allow us to construct high-order schemes for both the phase variable ϕ and ψ while only using a first-order approximation of the energy balance equation. To our knowledge, there is no careful research to give high-order accurate but energy stable schemes for the MPFC model. Meanwhile, the proposed approach only needs to solve linear equation with constant coefficients in one time step which is easy to use fast Fourier transform (FFT) to save more CPU time in calculation. Some numerical simulations are demonstrated to verify the accuracy and efficiency of our proposed schemes.

Keywords Modified phase field crystal model · SAV approach · High-order schemes · Numerical simulations

Mathematics Subject Classification (2010) 65M12; 35K20; 35K35; 35K55; 65Z05

✉ Zhengguang Liu
  liuzhgsdu@yahoo.com

Extended author information available on the last page of the article

1 Introduction

The modified phase field crystal (MPFC) model is a sixth-order evolutive nonlinear partial differential equation which was proposed in [18]. Compared with the traditional PFC model, the modified model can distinguish between the elastic relaxation and diffusion time scales [1]. For the MPFC model, perturbations are transmitted by waves that travel essentially undamped up to a certain length scale determined by the parameters. When this length scale is of the order of the size of the system, a separation of elastic relaxation and diffusion time scales may be practically observed [18]. Meanwhile, the MPFC model can still keep the original properties to describe many crystal phenomena such as edge dislocations [3], deformation and plasticity in nanocrystalline materials [19], FCC ordering [22], epitaxial growth and zone refinement [5]. The MPFC model is no longer a gradient flow. However, one can add a kinetic energy term to the original energy E of the PFC model to construct a pseudo-energy. In practice, we often regard the MPFC model as a pseudo-gradient flow. In general, we consider the following MPFC model:

$$\phi_{tt} + \beta\phi_t = M\Delta[\phi^3 - \epsilon\phi + (1+\Delta)^2\phi], \quad \text{in } Q \times \Omega, \tag{1.1}$$

with periodic boundary conditions and the following initial conditions:

$$\phi(0, \mathbf{x}) = \phi_0(\mathbf{x}), \quad \phi_t(0, \mathbf{x}) = \psi_0(\mathbf{x}), \quad \mathbf{x} \in \Omega.$$

The unknown function ϕ is the atomic density field. M is the mobility constant and $\epsilon > 0$ is a constant with physical significance. $\beta > 0$ is a relaxation parameter. $Q = (0,T]$ with $T > 0$.

In this paper, we focus on the numerical methods for the MPFC model. Similar to other phase field models, the scholars hope to construct energy stable numerical schemes for MPFC model. Many popular energy preserving methods such as convex splitting methods [1, 2, 7, 17, 20], stabilized methods [23, 25], invariant energy quadratization (IEQ) approach [8, 12, 27], scalar auxiliary variable (SAV) approach [9, 21, 24, 28] and so on are considered to discretize and simulate the MPFC model. It is worth mentioning that IEQ and SAV approaches are two very efficient and popular energy stable methods to construct linear, second-order numerical schemes. Recently, a new SAV approach is considered in [6] by Huang, Shen and Yang to construct high-order unconditionally stable adaptive time-stepping backward differentiation formula schemes. In this paper, we will apply this technique for the MPFC model. For more details about extensions and improvements of IEQ and SAV methods, we refer interested readers to the references [4, 10, 13, 14, 16].

The PFC-type equation is derived from the following Swift-Hohenberg type free energy functional

$$E(\phi) = \int_{\Omega} \left\{ \frac{1}{4}\phi^4 + \frac{1-\epsilon}{2}\phi^2 - |\nabla\phi|^2 + \frac{1}{2}(\Delta\phi)^2 \right\} d\mathbf{x}. \tag{1.2}$$

By introducing the chemical potential μ which is defined as

$$\mu = \frac{\delta E}{\delta \phi} = \phi^3 - \epsilon \phi + (1 + \Delta)^2 \phi, \tag{1.3}$$

one can rewrite the MPFC model (1.1) as follows

$$\phi_{tt} + \beta \phi_t = M \Delta \mu, \quad \text{in } Q \times \Omega. \tag{1.4}$$

It can be observed that (1.4) is not precisely a mass conservation equation due to the term ϕ_{tt}. In [8], we can find that if the initial condition satisfies $\int_\Omega \phi_0 d\mathbf{x} = 0$, the following mass conservation will hold:

$$\int_\Omega \phi_t(t, \mathbf{x}) d\mathbf{x} = \int_\Omega \phi_{tt}(t, \mathbf{x}) d\mathbf{x} = 0. \tag{1.5}$$

To derive the energy dissipation law, we need to define the H_{per}^{-1} inner product [8]. Suppose $u \in L_0^2(\Omega) = \{v \in L^2(\Omega) | (v, 1) = 0\}$, define $g_u \in H_{per}^2(\Omega) \cap L_0^2(\Omega)$ to be the unique solution to the following problem with periodic boundary condition:

$$-\Delta g_u = u \quad \text{in } \Omega. \tag{1.6}$$

We then define $g_u := (-\Delta)^{-1} u$, and for any $u, v \in L_0^2(\Omega)$, the H_{per}^{-1} inner product and norm can be defined as follows:

$$(u, v)_{-1} = (\nabla g_u, \nabla g_v), \quad \|u\|_{-1} = \sqrt{(u, u)_{-1}}. \tag{1.7}$$

It is easy to obtain the following identity:

$$(u, v)_{-1} = ((-\Delta)^{-1} u, v) = (u, (-\Delta)^{-1} v) = (v, u)_{-1}. \tag{1.8}$$

From [8], one can see that the MPFC model has the following energy dissipation law

$$\frac{d}{dt} E(\phi) = -\frac{\beta}{M} \|\phi_t\|_{-1}^2 \leq 0, \tag{1.9}$$

where the pseudo-energy $E(\phi)$ is defined as

$$E(\phi) = \int_\Omega \left\{ \frac{1}{4} \phi^4 + \frac{1 - \epsilon}{2} \phi^2 - |\nabla \phi|^2 + \frac{1}{2} (\Delta \phi)^2 \right\} d\mathbf{x} + \frac{1}{2M} \|\phi_t\|_{-1}^2, \tag{1.10}$$

The main purpose of this paper is to derive linear, energy dissipative and high-order accurate SAV-type schemes for the MPFC model. Partially inspired by the idea of the new scalar auxiliary variable (nSAV) approach introduced in [6], we propose the nSAV approach to construct high-order unconditional energy stable schemes based on the k-step backward differentiation formula (BDFk) to simulate the MPFC model. The considered nSAV schemes allow us to construct high-order schemes for both the phase variable ϕ and ψ while only using a first-order approximation of the energy balance equation. To our knowledge, there is no careful research to give high-order accurate but energy stable schemes for the MPFC model. Meanwhile, the

proposed approach only needs to solve linear equation with constant coefficients in one time step which is easy to use fast Fourier transform (FFT) to save more CPU time in calculation. We give some numerical examples in 2D and 3D to verify the accuracy and efficiency of our proposed schemes.

The paper is organized as follows. In Section 2, we give a brief summary of the classic SAV scheme for the time integration for the MPFC model. Then, our first-order nSAV scheme and the high-order schemes based on the k-step BDF are presented in Section 3, together with the energy dissipation law. Finally, in Section 4, various 2D and 3D numerical simulations are demonstrated to verify the accuracy and efficiency of our proposed schemes.

Before giving the discrete formulation, we let $N > 0$ be a positive integer and set

$$\Delta t = T/N, \quad t^n = n\Delta t, \quad \text{for} \quad n \le N.$$

2 The traditional SAV approach

Firstly, we will give a brief introduction of the traditional SAV scheme for the MPFC model. The detailed discretization form and analysis can be seen in [8]. Assume that there is a positive constant C to ensure $E_1(\phi) + C > 0$ where $E_1(\phi) = \int_\Omega F(\phi)d\mathbf{x} = \int_\Omega \frac{1}{4}\phi^4 - \frac{\epsilon}{2}\phi^2 d\mathbf{x}$ is a nonlinear energy functional. Then, we introduce a new variable ψ and a new SAV $r(t)$ as follows:

$$\psi = \phi_t, \quad r(t) = \sqrt{E_1(\phi) + C}. \tag{2.1}$$

Combining the above two new variables with the MPFC model (1.4), we can obtain the following equivalent MPFC system:

$$\begin{cases} \psi_t + \beta\psi = M\Delta\mu, \\ \quad \mu = (1 + \Delta)^2\phi + \dfrac{r(t)}{\sqrt{E_1(\phi) + C}}F'(\phi), \\ \quad \psi = \phi_t, \\ \quad r_t = \dfrac{1}{2\sqrt{E_1(\phi) + C}}(F'(\phi), \phi_t). \end{cases} \tag{2.2}$$

The new equivalent system follows a modified energy dissipative law:

$$\frac{d}{dt}\widehat{E}(\phi, q) = -\frac{\beta}{M}\|\psi\|_{-1}^2 \le 0, \tag{2.3}$$

where the modified energy $\widehat{E}(\phi, r)$ is defined as

$$\widehat{E}(\phi, r) = \int_\Omega \left\{\frac{1}{2}\phi(1 + \Delta)^2\phi\right\}d\mathbf{x} + r^2 - C|\Omega| + \frac{1}{2M}\|\psi\|_{-1}^2. \tag{2.4}$$

For the SAV-based time discretization schemes, we only give the following first-order scheme derived by the backward Euler method:

$$\begin{cases} \dfrac{\psi^{n+1} - \psi^n}{\Delta t} + \beta \psi^{n+1} = M\Delta\mu^{n+1}, \\ \qquad\qquad \mu^{n+1} = \dfrac{r^{n+1}}{\sqrt{E_1(\phi^n) + C}} F'(\phi^n) + (1 + \Delta)^2 \phi^{n+1}, \\ \qquad\qquad \psi^{n+1} = \dfrac{\phi^{n+1} - \phi^n}{\Delta t}, \\ \quad r^{n+1} - r^n = \dfrac{1}{2\sqrt{E_1(\phi^n) + C}} (F'(\phi^n), \phi^{n+1} - \phi^n). \end{cases} \qquad (2.5)$$

Theorem 2.1 The first-order SAV-based scheme (2.5) for the equivalent MPFC system (2.2) is unconditionally energy stable in the sense that

$$\frac{1}{\Delta t}\left[E^{n+1} - E^n\right] \le -\frac{\beta}{M}\|\psi^{n+1}\|_{-1}^2 \le 0,$$

where the modified discrete version of the energy is defined by

$$E^n = \frac{1}{2}\|(1 + \Delta)\phi^n\|^2 + \frac{1}{2M}\|\psi^n\|_{-1}^2 + (r^n)^2 - C|\Omega|.$$

3 Numerical new SAV schemes for MPFC model

In this section, we will give a series of numerical time-marching high-order schemes by using the new SAV approach for the MPFC model.

3.1 The first-order new SAV scheme

In this subsection, we will introduce a new SAV approach for the MPFC model to construct first-order semi-implicit energy stable schemes. Introduce a new scalar auxiliary variable:

$$R(t) = E(\phi) + C_0, \qquad (3.1)$$

where C_0 is a chosen scalar such that $E(\phi) + C_0 > 0$. Then, the following dynamical equation will be satisfied:

$$\frac{dR}{dt} = \frac{dE}{dt} = -\frac{\beta}{M}\|\phi_t\|_{-1}^2 = -\frac{\beta}{M}(\psi, \psi)_{-1} = -\frac{\beta}{M}(\nabla g_\psi, \nabla g_\psi) \le 0. \qquad (3.2)$$

Define $\xi(t) = \dfrac{R(t)}{E(\phi) + C_0}$ and note that $\xi(t) \equiv 1$ at the continuous level, then we can rewrite the MPFC model (2.2) as the following equivalent form:

$$\begin{cases} \psi_t + \beta\psi = M\Delta\mu, \\ \qquad \mu = (1+\Delta)^2\phi + U(\xi)F'(\phi) \\ \qquad \xi(t) = \dfrac{R(t)}{E(\phi)+C_0}, \\ \qquad \psi = \phi_t, \\ \qquad \dfrac{dR}{dt} = -\dfrac{\beta}{M}\xi(\nabla g_\psi, \nabla g_\psi), \end{cases} \tag{3.3}$$

where $U(\xi)$ is a specific function of ξ which satisfies $U(\xi) \equiv 1$ at the continuous level.

Firstly, set $U(\xi) = \xi(2-\xi)$, then our new first-order scheme for (3.3) is as follows:

$$\begin{cases} \dfrac{\psi^{n+1} - U(\xi^{n+1})\psi^n}{\Delta t} + \beta\psi^{n+1} = M\Delta\mu^{n+1}, \\ \qquad \mu^{n+1} = (1+\Delta)^2\phi^{n+1} + U(\xi^{n+1})F'(\phi^n), \\ \qquad \xi^{n+1} = \dfrac{R^{n+1}}{E(\overline{\phi}^{n+1})+C_0}, \\ \qquad \psi^{n+1} = \dfrac{\phi^{n+1} - U(\xi^{n+1})\phi^n}{\Delta t}, \\ \qquad \dfrac{R^{n+1} - R^n}{\Delta t} = -\dfrac{\beta}{M}\xi^{n+1}(\nabla g_{\overline{\psi}^{n+1}}, \nabla g_{\overline{\psi}^{n+1}}), \end{cases} \tag{3.4}$$

where $\overline{\phi}^{n+1}$ in the third equation and $\overline{\psi}^{n+1}$ in the fifth equation can be obtained as below. Given the initial conditions $\phi^0 = \phi_0$, $\psi^0 = \psi_0$ and $R^0 = E(\phi_0) + C_0$, one can obtain the following linear equation:

$$\big[(1+\Delta t\beta)I - M\Delta t^2\Delta(1+\Delta)^2\big]\psi^{n+1} = U(\xi^{n+1})\big[\psi^n + M\Delta t\Delta(1+\Delta)^2\phi^n + M\Delta t\Delta F'(\phi^n)\big]. \tag{3.5}$$

Setting

$$\psi^{n+1} = U(\xi^{n+1})\overline{\psi}^{n+1}, \quad \overline{\psi}^{n+1} = \dfrac{\overline{\phi}^{n+1} - \phi^n}{\Delta t}, \tag{3.6}$$

then substituting the first equation in (3.6) into the (3.5), we can find that $\overline{\psi}^{n+1}$ is determined by

$$\big[(1+\Delta t\beta)I - M\Delta t^2\Delta(1+\Delta)^2\big]\overline{\psi}^{n+1} = \big[\psi^n + M\Delta t\Delta(1+\Delta)^2\phi^n + M\Delta t\Delta F'(\phi^n)\big], \tag{3.7}$$

which means $\overline{\psi}^{n+1}$ can be solved explicitly. It is obviously to see that $\overline{\psi}^{n+1}$ can be viewed as an approximation of $\psi(t^{n+1})$ by a first-order semi-implicit method. Thus, $\overline{\psi}^{n+1}$ will be first-order approximation of $\psi(t^{n+1})$. Then, $(\nabla g_{\overline{\psi}^{n+1}}, \nabla g_{\overline{\psi}^{n+1}})$ can be obtained by $\overline{\psi}^{n+1}$. We are easy to obtain $\overline{\phi}^{n+1}$ by the second equation in (3.6):

$$\overline{\phi}^{n+1} = \phi^n + \Delta t\overline{\psi}^{n+1}.$$

Combining the third equation with the fifth equation in (3.4), we can compute ξ^{n+1} as follows:

$$\xi^{n+1} = \frac{MR^n}{ME(\overline{\phi}^{n+1}) + MC_0 + \Delta t \beta (\nabla g_{\overline{\psi}^{n+1}}, \nabla g_{\overline{\psi}^{n+1}})}. \tag{3.8}$$

Then ψ^{n+1} and ϕ^{n+1} can be obtained as follows:

$$\psi^{n+1} = U(\xi^{n+1})\overline{\psi}^{n+1}, \quad \phi^{n+1} = \Delta t \psi^{n+1} + U(\xi^{n+1})\phi^n. \tag{3.9}$$

Noting that $R^{n+1} = R(t^{n+1}) + O(\Delta t) = 1 + O(\Delta t)$, we then obtain

$$\xi^{n+1} = \xi(t^{n+1}) + C_1 \Delta t = 1 + C_1 \Delta t.$$

Noting that $U(\xi) = \xi(2 - \xi)$, which means that

$$1 - U(\xi^{n+1}) = 1 - \xi^{n+1}(2 - \xi^{n+1}) = 1 - (1 + C_1 \Delta t)(1 - C_1 \Delta t) = C_1^2 \Delta t^2.$$

Thus, we can easily obtain that

$$\frac{\psi^{n+1} - U(\xi^{n+1})\psi^n}{\Delta t} = \frac{\psi^{n+1} - \psi^n}{\Delta t} + \frac{[1 - U(\xi^{n+1})]\psi^n}{\Delta t} = \frac{\partial \psi}{\partial t}\bigg|^{n+1} + O(\Delta t). \tag{3.10}$$

Similarly, we immediately obtain

$$\frac{\phi^{n+1} - U(\xi^{n+1})\phi^n}{\Delta t} = \frac{\partial \phi}{\partial t}\bigg|^{n+1} + O(\Delta t). \tag{3.11}$$

To summarize, the first-order scheme (3.4) can be implemented as follows:

- compute $\overline{\psi}^{n+1}$ from the linear (3.7) by using the known ϕ^n and ψ^n;
- compute $\nabla g_{\overline{\psi}^{n+1}}$ to obtain $(\nabla g_{\overline{\psi}^{n+1}}, \nabla g_{\overline{\psi}^{n+1}})$ and $\overline{\phi}^{n+1} = \phi^n + \Delta t \overline{\psi}^{n+1}$;
- compute ξ^{n+1} from (3.8) and update $R^{n+1} = \xi^{n+1}(E(\overline{\phi}^{n+1}) + C_0)$;
- update $\psi^{n+1} = U(\xi^{n+1})\overline{\psi}^{n+1}$ and $\phi^{n+1} = \Delta t \psi^{n+1} + U(\xi^{n+1})\phi^n$ and go to the next time step.

By introducing $\overline{\psi}^{n+1}$, the unknown variables ξ^{n+1}, ψ^{n+1} and ϕ^{n+1} can be solved step-by-step which means that the above procedure only requires solving one linear equation with constant coefficients as in the standard semi-implicit scheme. As for the energy stability, we have the following theorem.

Theorem 3.1 $R^{n+1} > 0$ for any $n > 0$ and the first-order new SAV scheme (3.4) for the equivalent MPFC system (3.3) is unconditionally energy stable in the sense that

$$R^{n+1} - R^n = -\frac{\beta \Delta t}{M} \xi^{n+1} (\nabla g_{\overline{\psi}^{n+1}}, \nabla g_{\overline{\psi}^{n+1}}) \leq 0.$$

Proof Using the definition of $R(t)$, we can obtain $R^0 = E(\phi^0) + C_0 > 0$. Assuming that $R^n > 0$ for all $n = 1, 2, \ldots, k$. Next we only need to prove $R^{k+1} > 0$. From the (3.8), we obtain

$$\xi^{k+1} = \frac{MR^k}{ME(\overline{\phi}^{n+1}) + MC_0 + \Delta t \beta (\nabla g_{\overline{\psi}^{k+1}}, \nabla g_{\overline{\psi}^{k+1}})} > 0. \tag{3.12}$$

and noting $R^{k+1} = \xi^{k+1}(E(\overline{\phi}^{k+1}) + C_0)$, we are easy to obtain $R^{k+1} > 0$. Thus, we immediately obtain

$$R^{n+1} - R^n = -\frac{\beta \Delta t}{M} \xi^{n+1} (\nabla g_{\overline{\psi}^{n+1}}, \nabla g_{\overline{\psi}^{n+1}}) \le 0.$$

3.2 The high-order new SAV scheme

In this subsection, we will consider the high-order new SAV schemes for the MPFC model based on the k-step backward differentiation formula (BDFk). The essential idea is that we only need a first-order approximations for R and ξ to achieve overall k th-order accuracy for ϕ and ψ by using a $(k+1)$-order approximation of 1 for $U(\xi)$.

For the k th-order BDF new SAV scheme of the MPFC model, we set $U(\xi) = U_k(\xi)$. Then, couple with k-step backward differentiation formula, the high-order unconditionally energy stable new SAV schemes for the equivalent system (3.3) can be constructed as follows:

$$\begin{cases} \dfrac{\alpha \psi^{n+1} - U_k(\xi^{n+1})\widehat{\psi}^n}{\Delta t} + \beta \psi^{n+1} = M\Delta \mu^{n+1}, \\ \qquad\qquad \mu^{n+1} = (1+\Delta)^2 \phi^{n+1} + U_k(\xi^{n+1})F'(\phi^{*,n+1}), \\ \qquad\qquad \xi^{n+1} = \dfrac{R^{n+1}}{E(\overline{\phi}^{n+1}) + C_0}, \\ \qquad\qquad \psi^{n+1} = \dfrac{\alpha \phi^{n+1} - U_k(\xi^{n+1})\widehat{\phi}^n}{\Delta t}, \\ \dfrac{R^{n+1} - R^n}{\Delta t} = -\dfrac{\beta}{M} \xi^{n+1}(\nabla g_{\overline{\psi}^{n+1}}, \nabla g_{\overline{\psi}^{n+1}}), \end{cases} \tag{3.13}$$

where $U_k(\xi^{n+1})$ is a $k+1$-order approximation of 1. There are many ways to achieve $(k+1)$th-order convergent scheme for $1 - U(\xi)$. For example, we can choose

$$U_k(\xi) = 1 - (1-\xi)^{k+1}. \tag{3.14}$$

In (3.13), $\alpha, \widehat{\psi}^n, \widehat{\phi}^n$ and $\phi^{*,n+1}$ are defined as follows: BDF2:

$$\alpha = \frac{3}{2}, \quad \widehat{\psi}^n = 2\psi^n - \frac{1}{2}\psi^{n-1}, \quad \widehat{\phi}^n = 2\phi^n - \frac{1}{2}\phi^{n-1}, \quad \phi^{*,n+1} = 2\phi^n - \phi^{n-1}. \tag{3.15}$$

BDF3:

$$\alpha = \frac{11}{6}, \quad \widehat{\psi}^n = 3\psi^n - \frac{3}{2}\psi^{n-1} + \frac{1}{3}\psi^{n-2}, \quad \widehat{\phi}^n = 3\phi^n - \frac{3}{2}\phi^{n-1} + \frac{1}{3}\phi^{n-2}, \quad \phi^{*,n+1} = 3\phi^n - 3\phi^{n-1} + \phi^{n-2}.$$

(3.16)

BDF4:

$$\alpha = \frac{25}{12}, \quad \widehat{\psi}^n = 4\psi^n - 3\psi^{n-1} + \frac{4}{3}\psi^{n-2} - \frac{1}{4}\psi^{n-3}, \quad \widehat{\phi}^n = 4\phi^n - 3\phi^{n-1} + \frac{4}{3}\phi^{n-2} - \frac{1}{4}\phi^{n-3},$$
$$\phi^{*,n+1} = 4\phi^n - 6\phi^{n-1} + 4\phi^{n-2} - \phi^{n-3}.$$

(3.17)

Doting that $1 - U(\xi^{n+1}) = O(\Delta t^{k+1})$, we can directly observe that

$$\frac{\alpha\psi^{n+1} - U_k(\xi^{n+1})\widehat{\psi}^n}{\Delta t} = \frac{\alpha\psi^{n+1} - \widehat{\psi}^n}{\Delta t} + \frac{[1 - U_k(\xi^{n+1})]\widehat{\psi}^n}{\Delta t} = \left.\frac{\partial\psi}{\partial t}\right|^{n+1} + O(\Delta t^k).$$

(3.18)

The above high-order BDFk schemes also enjoy the same stability as the first-order scheme (3.16).

Theorem 3.2 $R^{n+1} > 0$ and $\xi^{n+1} > 0$ for any $n > 0$ and the BDFk schemes (3.13)–(3.17) for $k = 2,3,4$ are all unconditionally energy stable in the sense that

$$R^{n+1} - R^n = -\frac{\beta\Delta t}{M}\xi^{n+1}(\nabla g_{\overline{\psi}^{n+1}}, \nabla g_{\overline{\psi}^{n+1}}) \leq 0.$$

By introducing an intermediate variable $\overline{\psi}^{n+1}$, the unknown variables $\overline{\phi}^{n+1}$, ξ^{n+1}, R^{n+1}, ψ^{n+1} and ϕ^{n+1} can also be solved step-by-step as the first-order scheme (3.16) which means that the above procedure only requires solving one linear equation with constant coefficients as in the standard semi-implicit scheme. By introducing $\overline{\psi}^{n+1}$ to satisfy $\psi^{n+1} = U_k(\xi^{n+1})\overline{\psi}^{n+1}$, we can rewrite the scheme (3.13) as follows:

$$\begin{cases} \dfrac{\alpha\overline{\psi}^{n+1} - \widehat{\psi}^n}{\Delta t} + \beta\overline{\psi}^{n+1} = \dfrac{M}{\alpha}\Delta(1+\Delta)^2(\Delta t\psi^{n+1} + \widehat{\phi}^n) + M\Delta F'(\phi^{*,n+1}), \\[2mm] \xi^{n+1} = \dfrac{R^{n+1}}{E(\overline{\phi}^{n+1}) + C_0}, \\[2mm] \dfrac{R^{n+1} - R^n}{\Delta t} = -\dfrac{\beta}{M}\xi^{n+1}(\nabla g_{\overline{\psi}^{n+1}}, \nabla g_{\overline{\psi}^{n+1}}), \\[2mm] \psi^{n+1} = U_k(\xi^{n+1})\overline{\psi}^{n+1}. \end{cases}$$

(3.19)

Actually, it is not difficult to find that the nSAV BDFk scheme (3.19) can be divided into the following five steps:

Step I: Compute $\overline{\psi}^{n+1}$ by the following semi-implicit BDFk scheme:

$$\left[(\alpha + \Delta t\beta)I - \frac{M\Delta t^2}{\alpha}\Delta(1+\Delta)^2\right]\overline{\psi}^{n+1} = \widehat{\psi}^n + \frac{M\Delta t}{\alpha}\Delta(1+\Delta)^2\widehat{\phi}^n + M\Delta t\Delta F'(\phi^{*,n+1}).$$

(3.20)

Step II: Compute $(\nabla g_{\overline{\psi}^{n+1}}, \nabla g_{\overline{\psi}^{n+1}})$ and $\overline{\phi}^{n+1}$ by the known $\overline{\psi}^{n+1}$ and the following scheme:

$$(\nabla g_{\overline{\psi}^{n+1}}, \nabla g_{\overline{\psi}^{n+1}}) = \|\overline{\psi}^{n+1}\|_{-1}, \quad \overline{\phi}^{n+1} = \phi^n + \Delta t \overline{\psi}^{n+1}. \tag{3.21}$$

Step III: Compute ξ^{n+1} and R^{n+1} by the known $\overline{\psi}^{n+1}$ and the following scheme:

$$\xi^{n+1} = \frac{MR^n}{ME(\overline{\phi}^{n+1}) + MC_0 + \Delta t\beta(\nabla g_{\overline{\psi}^{n+1}}, \nabla g_{\overline{\psi}^{n+1}})}, \quad R^{n+1} = \xi^{n+1}(E(\overline{\phi}^{n+1}) + C_0). \tag{3.22}$$

Step IV: Using $\overline{\psi}^{n+1}$, and $U_k(\xi^{n+1})$ to obtain ψ^{n+1},:

$$\psi^{n+1} = U_k(\xi^{n+1})\overline{\psi}^{n+1}. \tag{3.23}$$

Step V: Compute ϕ^{n+1} by the following equation:

$$\phi^{n+1} = \frac{1}{\alpha}\left(\Delta t\psi^{n+1} + U_k(\xi^{n+1})\hat{\phi}^n\right). \tag{3.24}$$

4 Numerical experiments

In this section, we will give some numerical examples to simulate the MPFC model in 2D and 3D to test our theoretical analysis which contain energy stability and convergence rates of the proposed high-order nSAV schemes. In all examples, we consider the periodic boundary conditions and use a Fourier spectral method in space.

4.1 Convergence test

Firstly, we give the following example 1 to verify the convergence order in time for the proposed high-order nSAV schemes.

Example 1 The initial value is given by

$$\phi(x, y, t) = 0.01 \sin(\frac{2\pi x}{64}) \cos(\frac{2\pi y}{64}). \tag{4.1}$$

The computational domain can be set as $\Omega = [0,128] \times [0,128]$. The parameters are $\epsilon = 0.025$, $\beta = 0.9$, $M = 1$, $T = 0.1$ and $C_0 = 1$. We discretize the space by the Fourier spectral method with 256×256 modes. Given the analytical solutions are unknown, we take the mesh refinement test by choosing the numerical solution with $\Delta t = 1 \times 10^{-5}$ as the analytical solution for computing errors. Firstly, we list the $l^\infty(L^2)$ errors and convergence rates of the phase variable ϕ and the introduced auxiliary variables ξ and ψ between the numerical solution and the approximate solution at $T = 0.1$ with different time step sizes in Tables 1, 2, 3, and 4. We can observe that the expected convergence rates of the field variable ϕ and the introduced variable ψ match their corresponding orders for all cases. For the high-order BDFk (k = 2; 3; 4) nSAV schemes, we can achieve overall k th-order accuracy for ϕ and ψ by using just a first-order approximation for ξ if we choose proper $U(\xi)$ such

Table 1 The errors, convergence rates and CPU time in time for the first-order scheme of example 1

Δt	$\|e_\phi\|_{l^\infty(L^2)}$		$\|e_\psi\|_{l^\infty(L^2)}$		$\|e_\xi\|_{l^\infty(L^2)}$		
	Error	Rate	Error	Rate	Error	Rate	CPU time
4×10^{-3}	2.0680e-4	–	1.6349e-5	–	5.5352e-2	–	1.46
2×10^{-3}	1.0385e-4	0.9938	8.1161e-6	1.0103	2.8403e-2	0.9626	2.61
1×10^{-3}	5.1844e-5	1.0022	4.0281e-6	1.0107	1.4395e-2	0.9805	5.12
5×10^{-4}	2.5706e-5	1.0121	1.9913e-6	1.0164	7.2475e-3	0.9900	9.82

Table 2 The errors, convergence rates and CPU time in time for the second-order scheme of example 1

Δt	$\|e_\phi\|_{l^\infty(L^2)}$		$\|e_\psi\|_{l^\infty(L^2)}$		$\|e_\xi\|_{l^\infty(L^2)}$		
	Error	Rate	Error	Rate	Error	Rate	CPU time
4×10^{-3}	3.6305e-6	–	2.8108e-7	–	3.0769e-2	–	1.43
2×10^{-3}	9.2247e-7	1.9766	7.0817e-8	1.9888	1.5437e-2	0.9951	2.67
1×10^{-3}	2.3246e-7	1.9885	1.7797e-8	1.9926	7.7335e-3	0.9972	5.41
5×10^{-4}	5.8331e-8	1.9946	4.4607e-9	1.9962	3.8708e-3	0.9985	10.08

Table 3 The errors, convergence rates and CPU time in time for the third-order scheme of example 1

Δt	$\|e_\phi\|_{l^\infty(L^2)}$		$\|e_\psi\|_{l^\infty(L^2)}$		$\|e_\xi\|_{l^\infty(L^2)}$		
	Error	Rate	Error	Rate	Error	Rate	CPU time
4×10^{-3}	1.0655e-7	–	8.5014e-9	–	3.0364e-2	–	1.91
2×10^{-3}	1.4363e-8	2.8912	1.1368e-9	2.9027	1.5343e-2	0.9848	2.57
1×10^{-3}	1.8628e-9	2.9468	1.4687e-10	2.9525	7.7111e-3	0.9926	5.07
5×10^{-4}	2.3716e-10	2.9735	1.8682e-11	2.9748	3.8653e-3	0.9963	10.07

Table 4 The errors, convergence rates and CPU time in time for the fourth-order scheme of example 1

Δt	$\|e_\phi\|_{l^\infty(L^2)}$		$\|e_\psi\|_{l^\infty(L^2)}$		$\|e_\xi\|_{l^\infty(L^2)}$		
	Error	Rate	Error	Rate	Error	Rate	CPU time
4×10^{-3}	2.9091e-9	–	2.3945e-10	–	2.9930e-2	–	1.28
2×10^{-3}	2.0790e-10	3.8066	1.7103e-11	3.8074	1.5237e-2	0.9740	2.59
1×10^{-3}	1.3883e-11	3.9045	1.2064e-12	3.8255	7.6849e-3	0.9875	5.23
5×10^{-4}	9.1030e-13	3.9308	7.7837e-14	3.9541	3.8588e-3	0.9939	10.12

that $U(\xi)$ is a $(k+1)$th-order approximation to 1. A first-order convergence for ξ is observed in Tables 2, 3, and 4 while such first-order convergence of ξ will not influence the expected convergence rates of ϕ and ψ. Besides, The CPU times shown in Tables 1, 2, 3, and 4 indicate that the proposed algorithm is very fast and efficient.

4.2 Energy stability test

In this subsection, the following example 2 is given to check the energy stability of the proposed nSAV schemes.

Example 2 The initial condition is taken as follows [9]

$$
\begin{aligned}
\phi(x, y, 0) =\ & 0.07 - 0.02 \cos\left(\tfrac{2\pi(x-12)}{32}\right) \sin\left(\tfrac{2\pi(y-1)}{32}\right) \\
& + 0.02 \cos^2\left(\tfrac{\pi(x+10)}{32}\right) \cos^2\left(\tfrac{\pi(y+3)}{32}\right) \\
& - 0.01 \sin^2\left(\tfrac{4\pi x}{32}\right) \sin^2\left(\tfrac{4\pi(y-6)}{32}\right).
\end{aligned}
$$

Set the computational domain as $\Omega = [0,128] \times [0,128]$ and the parameters $\epsilon = 0.025$, $M = 1$, $T = 100$ and $C_0 = 1$. We discretize the space by the Fourier spectral method with 256×256 modes. In Figs. 1 and 2, we plot the evolution of the original energy E defined in (1.2), the pseudo-energy E in (1.10), and the modified discrete energies $R - C_0$ in Theorem 3.2 with different β or Δt. In Fig. 1, we observe that the original energy E may increase on some time intervals. However, the pseudo-energy E and the modified energy $R - C_0$ are strictly dissipative in time. In Fig. 1, we give some different β to test the energy stability of the proposed schemes. When β is large, ϕ_t will become the main term in $\phi_{tt} + \beta\phi_t$, the MPFC model behaves like the traditional PFC model which leads the pseudo-energy E and the modified energy $R - C_0$ are nearly identical to the original energy E. However, for any different β, both pseudo-energy E and the modified energy $R - C_0$ are always non-increasing. The above numerical results are consistent with the results in [8]. We reset $T = 300$ to verify the dissipative properties of the proposed algorithm for long time simulation. Figure 2 presents the evolution of the modified discrete energies with different time step sizes of $\Delta t = 10$, 1 and 0.1 by using the second-order and third-order nSAV schemes. We observe that no matter big or small time step, the energies are strictly decay in time which indicates the proposed numerical schemes are unconditionally energy stable.
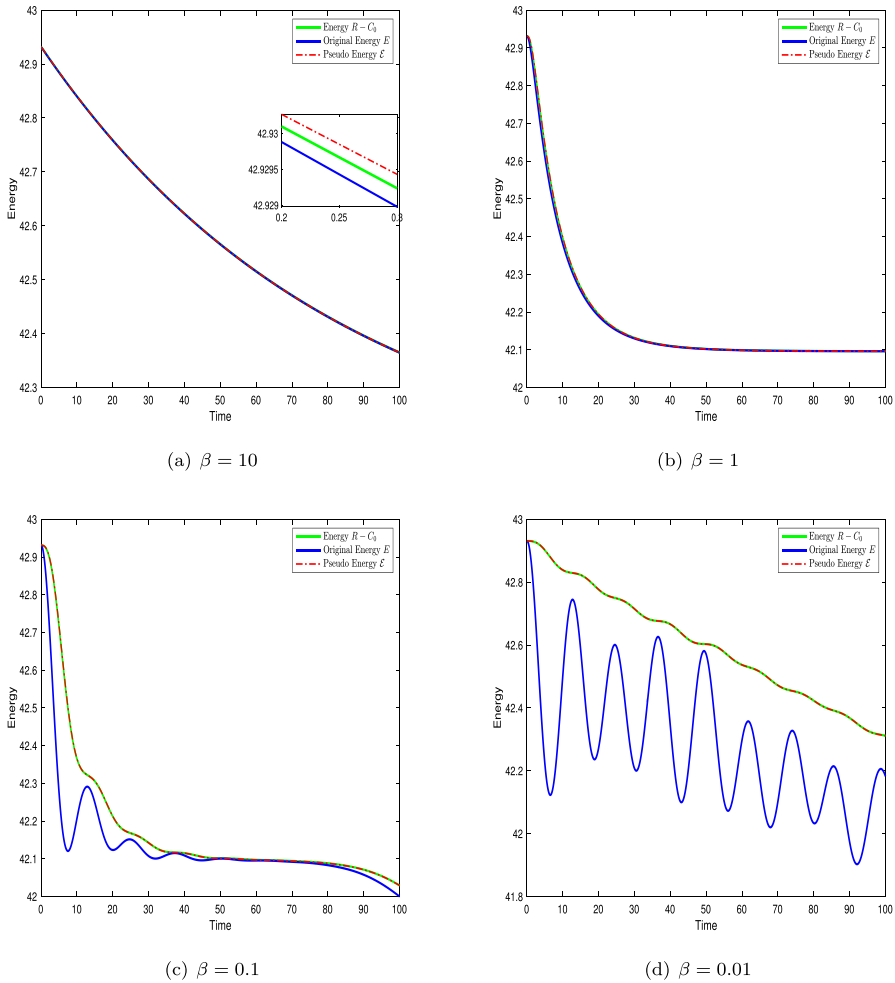
4.3 Phase transition behaviors

Next, we plan to simulate the phase transition behavior of the MPFC model in a supercooled liquid. The similar numerical examples can be found in many articles such as [11, 26, 29].

Example 3 The initial condition is

$$
\phi_0(x, y) = \bar{\phi} + \eta Rand(x, y), \quad \forall(x, y) \in \Omega. \tag{4.2}
$$

where the $Rand(x,y)$ is the random number in $[-1,1]$ with zero mean. In this example, we fix the parameter $\beta = 0.2$ and $\epsilon = 0.025$. The computational domain $\Omega =$

Fig. 1 Energy evolution of the second-order nSAV scheme for example 2 with $\beta = 10, 1, 0.1,$ and 0.01

$(0,128)^2$ and we discretize the space by the Fourier spectral method with 128×128 modes.

Set $\bar{\phi} = 0.07$ and $\eta = 0.07$. We show the phase transition behavior of the density field by using the second-order nSAV scheme with $\Delta t = 10^{-3}$ at various times in Fig. 3. The snapshots of the numerical approximation of ϕ at $t = 20, 70, 100, 200,$ 400 and 1000 are shown in Fig. 3. All of the numerical results are consistent with the transition behavior in some other researches such as [11, 26, 29]. We also investigate the effect of average of density field and ϵ. From Fig. 4, one can see that the increase of parameter ϵ will change the shape of the crystals.

For 3D simulation, we use 64^3 Fourier modes to discretize the 3D space. The time step is $\Delta t = 1$ and $\eta = 0.01$. The computational domain is $[0,50]^3$. The parameters

Fig. 2 Energy evolution of for example 2 with different time step Δt

(a) t=20

(b) t=70

(c) t=100

(d) t=200

(e) t=400

(f) t=1000
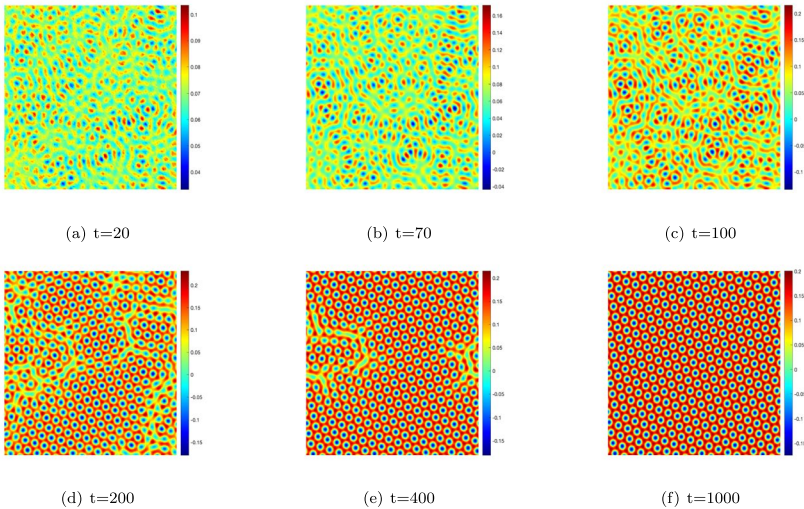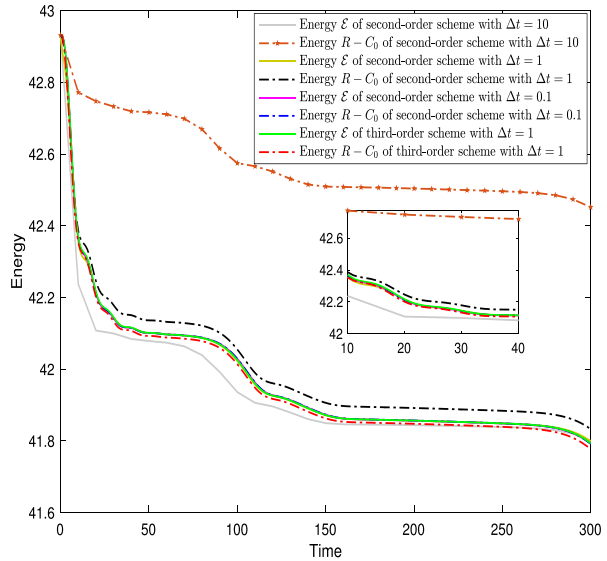
Fig. 3 Snapshots of the phase variable ϕ are taken at $t = 20, 70, 100, 200, 400$ and 1000 for example 3 with $\beta = 0.2$ and $\epsilon = 0.025$

are $\epsilon = 0.56$, $\beta = 0.1$, and $T = 4000$. Figure 5 presents the steady-state microstructure of the phase transition behavior with $\bar{\phi} = -0.20$, $\bar{\phi} = -0.35$ and $\bar{\phi} = -0.43$. We also give the CPU time for all BDFk nSAV schemes in Fig. 6 to show the high efficiency.

(a) t=5   (b) t=10   (c) t=15

(d) t=20   (e) t=40   (f) t=200
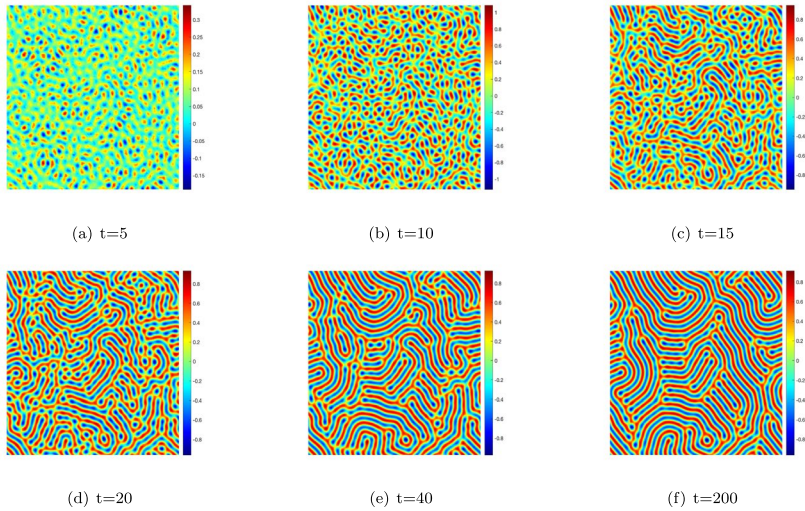
Fig. 4 Snapshots of the phase variable ϕ are taken at $t = 5$, 10, 15, 20, 40 and 200 for example 3 with $\beta = 0.25$ and $\epsilon = 0.4$

Example 4 In the following, we take $\epsilon = 0.25$, $\beta = 0.9$, $\Delta t = 0.1$ and $C_0 = 1$ to start our simulation on a domain $[0,600]^2$ with a 512×512 mesh grid by Fourier spectral method in space. We generated the three crystallites using random perturbations on three small square pathes. The following expression will be used to define the crystallites such as in [8]:

$$\phi(x_l, y_l) = \overline{\phi} + C\left(\cos(\frac{p}{\sqrt{3}}y_l)\cos(px_l) - \frac{1}{2}\cos(\frac{2p}{\sqrt{3}}y_l)\right),$$

where x_l, y_l define a local system of cartesian coordinates that is oriented with the crystallite lattice. The parameters $\overline{\phi} = 0.285$, $C = 0.446$ and $p = 0.66$. The local cartesian system is defined as

$$x_l(x, y) = x\sin\theta + y\cos\theta,$$
$$y_l(x, y) = -x\cos\theta + y\sin\theta.$$

The centers of three pathes are located at $(100,100)$, $(250,300)$ and $(300,200)$ with $\theta = \pi/4$, 0 and $-\pi/4$ and we set the length of each square to be 40. Figure 7 shows the snapshots of the density field ϕ at different times. One can observe that three different crystal grains grow from a supercooled liquid and become large enough to form grain boundaries finally.
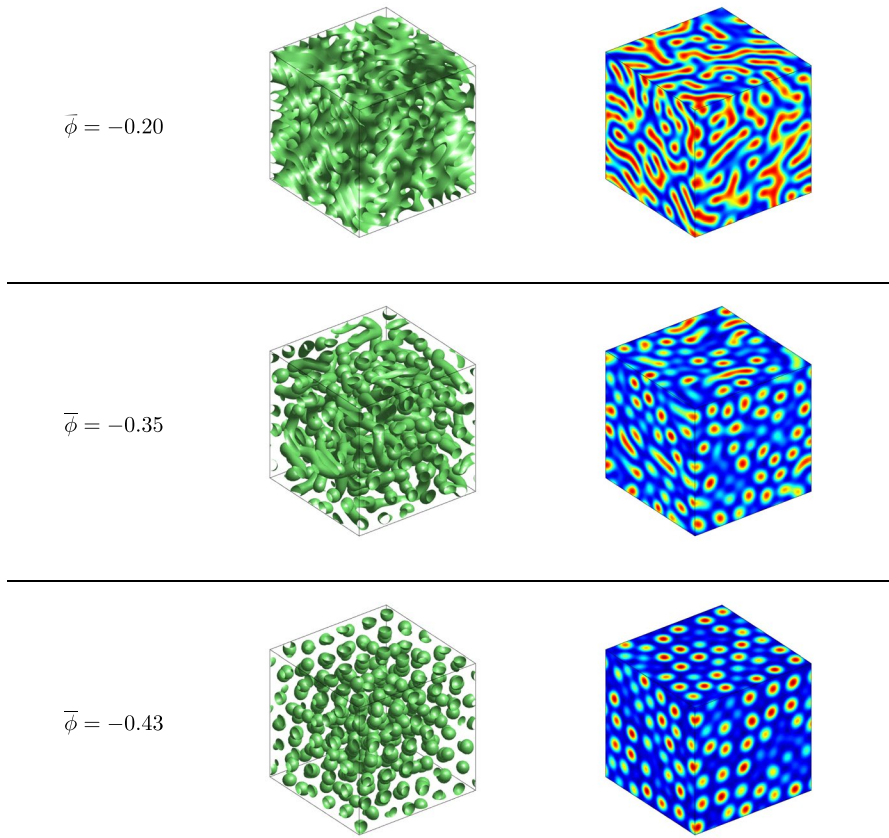
Fig. 5 The evolution of the phase transition behavior in 3D with different $\overline{\phi}$. The computational domain is $[0,50]^3$. The parameters are $\epsilon = 0.56$, $\beta = 0.1$, and $T = 4000$. 64^3 Fourier modes are used to discretize the space. The time step is $\Delta t = 1$. Left: isosurface plots of $\phi = 0$. Right: snapshots of the density field ϕ.

Example 5 In this example, we consider to simulate the growth of the crystalline phase in a 3D supercooled liquid on the computational domain $\Omega = [0,128]^3$ with 128^3 Fourier modes and the initial condition as

$$\phi(x, y, z, 0) = \begin{cases} 0.285 + 0.01\text{Rand}(x, y, z), & \sqrt{x^2 + (y - 26)^2 + (z + 44)^2} \leq 7 \\ & \text{or } \sqrt{x^2 + (y + 44)^2 + (z - 26)^2} \leq 7, \\ 0.285, & \text{else}, \end{cases}$$

(4.3)

where Rand(x,y,z) stands for the random values in $[-1,1]^3$. In Fig. 8, we plot slice diagrams (left) and isosurface diagrams (right) for the model for the model with $\Delta t = 1$, $\epsilon = 0.25$, $\beta = 0.9$, $C_0 = 10^5$. We observe similar numerical behavior as in the 2D case.

Fig. 6 The CPU time for the phase transition behavior in 3D with $\bar{\phi} = -0.43$

(a) t=0   (b) t=80   (c) t=150   (d) t=300

(e) t=400   (f) t=500   (g) t=600   (h) t=800
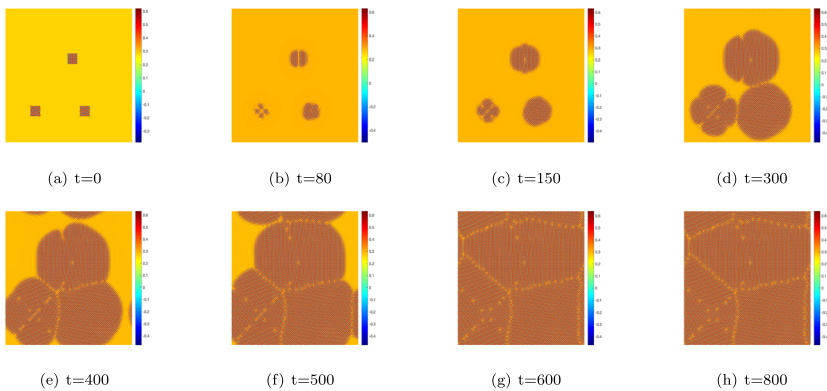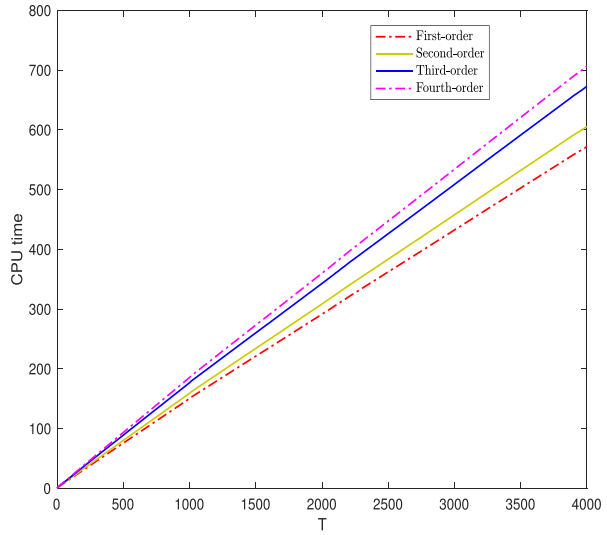
Fig. 7 Snapshots of the phase variable ϕ are taken at t = 0, 80, 150, 300, 400, 500, 600, 800 for example 3

5 Conclusion

In this paper, we consider linear, energy dissipative and high-order accurate SAV-type schemes for the MPFC model. A new SAV approach is proposed to construct high-order unconditional energy stable schemes based on the k-step backward differentiation formula (BDFk) to simulate the MPFC model. The proposed approach only needs to solve linear equation with constant coefficients in one time step which is easy to use fast Fourier transform (FFT) to save more CPU time in calculation. We give some numerical examples in 2D and 3D to verify the accuracy and efficiency of our proposed schemes. In future, we will consider some other efficient high-order SAV-type

(a) t=0   (b) t=600

(c) t=1000   (d) t=2000
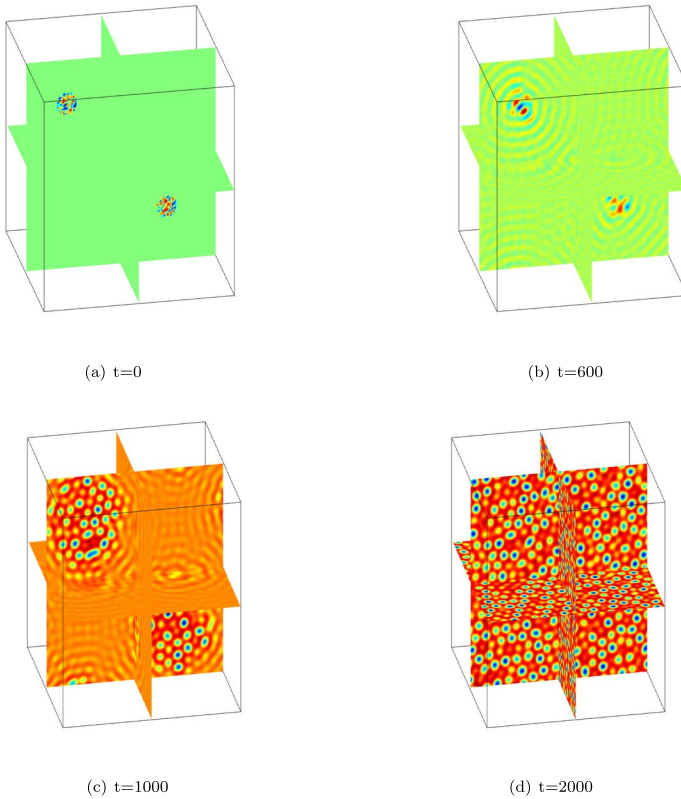
Fig. 8 The 3D dynamical behaviors of the crystal growth in a supercooled liquid. Snapshots of the numerical approximation of the density field ϕ are taken at t = 0, 600, 1000, 2000

approaches such as ESI-SAV method [15] to simulate the MPFC model and some other energy dissipative systems.

Declarations

Conflict of interest The authors declare no competing interests.

References

1. Baskaran, A., Hu, Z., Lowengrub, J.S., Wang, C., Wise, S.M., Zhou, P.: Energy stable and efficient finite-difference nonlinear multigrid schemes for the modified phase field crystal equation. J. Comput. Phys. **250**, 270–292 (2013)

2. Baskaran, A., Lowengrub, J.S., Wang, C., Wise, S.M.: Convergence analysis of a second order convex splitting scheme for the modified phase field crystal equation. SIAM J. Numer. Anal. **51**, 2851–2873 (2013)

3. Berry, J., Grant, M., Elder, K.R.: Diffusive atomistic dynamics of edge dislocations in two dimensions. Physical Review E Statistical Nonlinear & Soft Matter Physics **73**, 031609 (2006)

4. Cheng, Q., Liu, C., Shen, J.: A new lagrange multiplier approach for gradient flows. Comput. Methods Appl. Mech. Eng. **367**, 113070 (2020)

5. Elder, K.R., Katakowski, M., Haataja, M., Grant, M.: Modeling elasticity in crystal growth. Phys. Rev. Lett. **88**, 245701 (2002)

6. Huang, F., Shen, J., Yang, Z.: A highly efficient and accurate new scalar auxiliary variable approach for gradient flows. SIAM J. Sci. Comput. **42**, A2514–A2536 (2020)

7. Lee, H.G., Shin, J., Lee, J.-Y.: First-and second-order energy stable methods for the modified phase field crystal equation. Comput. Methods Appl. Mech. Eng. **321**, 1–17 (2017)

8. Li, Q., Mei, L., Yang, X., Li, Y.: Efficient numerical schemes with unconditional energy stabilities for the modified phase field crystal equation. Adv. Comput. Math. **45**, 1551–1580 (2019)

9. Li, X., Shen, J.: Efficient linear and unconditionally energy stable schemes for the modified phase field crystal equation. arXiv:2004.04319 (2020)

10. Li, X., Shen, J., Liu, Z.: New SAV-pressure correction methods for the Navier-Stokes equations: stability and error analysis. arXiv:2002.09090 (2020)

11. Li, Y., Kim, J.: An efficient and stable compact fourth-order finite difference scheme for the phase field crystal equation. Comput. Methods Appl. Mech. Eng. **319**, 194–216 (2017)

12. Liu, Z., Li, X.: Efficient modified stabilized invariant energy quadratization approaches for phase-field crystal equation. Numerical Algorithms **85**, 107–132 (2020)

13. Liu, Z., Li, X.: The exponential scalar auxiliary variable (e-SAV) approach for phase field models and its explicit computing. SIAM J. Sci. Comput. **42**, B630–B655 (2020)

14. Liu, Z., Li, X.: Two fast and efficient linear semi-implicit approaches with unconditional energy stability for nonlocal phase field crystal equation. Appl. Numer. Math. **150**, 491–506 (2020)

15. Liu, Z., Li, X.: A highly efficient and accurate exponential semi-implicit scalar auxiliary variable (esi-sav) approach for dissipative system. Journal of Computational Physics **447**, 110703 (2021)

16. Liu, Z., Li, X.: Step-by-step solving schemes based on scalar auxiliary variable and invariant energy quadratization approaches for gradient flows. Numerical Algorithms **89**, 65–86 (2022)

17. Shin, J., Lee, H.G., Lee, J.-Y.: First and second order numerical methods based on a new convex splitting for phase-field crystal equation. J. Comput. Phys. **327**, 519–542 (2016)

18. Stefanovic, P., Haataja, M., Provatas, N.: Phase-field crystals with elastic interactions. Phys. Rev. Lett. **96**, 225504 (2006)

19. Stefanovic, P.N.P., Haataja, M.: Phase field crystal study of deformation and plasticity in nanocrystalline materials. Phys. Rev. E **80**, 046107 (2009)

20. Wang, C., Wise, S. M.: An energy stable and convergent finite-difference scheme for the modified phase field crystal equation. SIAM J. Numer. Anal. **49**, 945–969 (2011)

21. Wang, M., Huang, Q., Wang, C.: A second order accurate scalar auxiliary variable (sav) numerical method for the square phase field crystal equation. J. Sci. Comput. **88**, 1–36 (2021)

22. Wu, K.-A., Adland, A., Karma, A.: Phase-field-crystal model for fcc ordering. Physical Review E Statistical Nonlinear & Soft Matter Physics **81**, 061601 (2010)

23. Xia, B., Mei, C., Yu, Q., Li, Y.: A second order unconditionally stable scheme for the modified phase field crystal model with elastic interaction and stochastic noise effect. Comput. Methods Appl. Mech. Eng. **363**, 112795 (2020)

24. Yang, J., Kim, J.: Energy dissipation–preserving time-dependent auxiliary variable method for the phase-field crystal and the swift–hohenberg models. Numerical Algorithms, pp. 1–30 (2021)

25. Yang, X.: Efficient linear, stabilized, second-order time marching schemes for an anisotropic phase field dendritic crystal growth model. Comput. Methods Appl. Mech. Eng. **347**, 316–339 (2019)

26. Yang, X., Han, D.: Linearly first-and second-order, unconditionally energy stable schemes for the phase field crystal model. J. Comput. Phys. **330**, 1116–1134 (2017)

27. Yang, X., Ju, L.: Efficient linear schemes with unconditional energy stability for the phase field elastic bending energy model. Comput. Methods Appl. Mech. Eng. **315**, 691–712 (2017)
28. Zhang, J., Yang, X.: Efficient second order unconditionally stable time marching numerical scheme for a modified phase-field crystal model with a strong nonlinear vacancy potential. Comput. Phys. Commun. **245**, 106860 (2019)
29. Zhang, J., Yang, X.: Numerical approximations for a new l2-gradient flow based phase field crystal model with precise nonlocal mass conservation. Comput. Phys. Commun. **243**, 51–67 (2019)

Authors and Affiliations

Zhengguang Liu[1] [iD] **· Nan Zheng[2] · Zhaojie Zhou[1]**

Nan Zheng
znan2017@163.com

Zhaojie Zhou
zhouzhaojie@sdnu.edu.cn

[1]   School of Mathematics and Statistics, Shandong Normal University, Jinan, China

[2]   School of Mathematical Sciences and Fujian Provincial Key Laboratory on Mathematical Modeling and High Performance Scientific Computing, Xiamen University, Xiamen, Fujian 361005, China